Materials Chemistry and Physics 191 (2017) 106–113

Contents lists available at ScienceDirect

Materials Chemistry and Physics

journal homepage: www.elsevier.com/locate/matchemphys

Advances on the synthesis of porous TiO_2 coatings by anodic spark oxidation. Photocatalytic reduction of Cr(VI)

Hernán D. Traid [a, b, c], María L. Vera [a, b, c], Alicia E. Ares [a, b, c], Marta I. Litter [b, d, e, *]

[a] Instituto de Materiales de Misiones, (CONICET-UNaM), Félix de Azara 1552, 3300, Posadas, Misiones, Argentina
[b] Consejo Nacional de Investigaciones Científicas y Técnicas, Godoy Cruz 2290, 1425, Ciudad Autónoma de Buenos Aires, Argentina
[c] Facultad de Ciencias Exactas, Químicas y Naturales, Universidad Nacional de Misiones, Félix de Azara 1552, 3300, Posadas, Misiones, Argentina
[d] Gerencia Química, Centro Atómico Constituyentes, Comisión Nacional de Energía Atómica, Av. Gral. Paz 1499, 1650, San Martín, Buenos Aires, Argentina
[e] Instituto de Investigación e Ingeniería Ambiental, Universidad Nacional de Gral San Martín, Campus Miguelete, Av. 25 de Mayo y Martín de Irigoyen, 1650, San Martín, Prov. de Buenos Aires, Argentina

HIGHLIGHTS

- Efficient porous TiO_2 anodic coatings were obtained in spark discharge conditions.
- Photocatalytic activity of TiO_2 anodic coatings was evaluated for Cr(VI)/EDTA.
- Higher electrolyte concentration and current density yield more active samples.
- The photocatalytic activity is related with the anatase fraction of the samples.
- A thermal treatment increases crystallinity and photocatalytic activity of samples.

ARTICLE INFO

Article history:
Received 11 May 2016
Received in revised form
18 December 2016
Accepted 9 January 2017
Available online 10 January 2017

Keywords:
TiO_2 coatings
Anodic oxidation
Cr(VI) reduction
Heterogeneous photocatalysis

ABSTRACT

Porous TiO_2 coatings were obtained by anodic oxidation in spark discharge conditions, varying the range of current density (200–3000 A m^{-2}) and the electrolyte concentration (H_2SO_4; 1 and 4 M). The samples were characterized by SEM, XRD and DRS. The photocatalytic activity was evaluated using the Cr(VI)/EDTA reductive system to find the optimal conditions for a high photocatalytic activity. A higher electrolyte concentration increased the pore diameter, the porous fraction and the coating thickness and, consequently, the photocatalytic activity; a higher current density improved the performance of coatings. A relationship between the anatase fraction and the photocatalytic activity of the samples was demonstrated, with a maximum activity close to 0.65 anatase fraction. The thermal treatment of the anodic coatings improved also the photocatalytic activity, without changes on neither the morphology nor the anatase fraction. The maximum Cr(VI) transformation achieved by the most active coating was 89.1% while a coating prepared with Evonik P25 achieved only 69.9%. The obtained TiO_2 anodic coatings present great potential for application in heterogeneous photocatalysis processes in water and wastewater treatment as supported photocatalysts.

1. Introduction

From the existing photocatalysts, TiO_2 is one of the most used materials due to its commercial availability, low cost, photostability and relatively high photocatalytic efficiency for water treatment [1]. Usually, TiO_2 is employed as a powder suspended in the polluted water. However, the use of particles involves the need of incorporating extra stages in the purification process, such as separation and catalyst recycling, which can be avoided by immobilizing TiO_2 as thin coatings onto different supports. Thin TiO_2 coatings have potential interest for self-cleaning and antifogging surfaces, and crystalline TiO_2 oxides (anatase and rutile) present very good photocatalytic behavior, superhydrophilicity and biocompatible properties [2,3]. The techniques used for obtaining TiO_2 coatings are very varied, being the anodic oxidation one of the simplest and most economical methods [4–7].

* Corresponding author. Gerencia Química, Centro Atómico Constituyentes, Comisión Nacional de Energía Atómica, Av. Gral. Paz 1499, 1650, San Martín, Buenos Aires, Argentina.
E-mail addresses: marta.litter@gmail.com, litter@cnea.gov.ar (M.I. Litter).

http://dx.doi.org/10.1016/j.matchemphys.2017.01.034
0254-0584/

In the anodic oxidation process, a direct current is circulated between a cathode and an anode immersed in an electrolyte solution, inducing reduction reactions in the cathode and oxidation reactions in the anode, where the material to be oxidized, e.g., titanium, is placed. Sulfuric acid is the most common electrolyte used in this technique [8]. Above a certain cell voltage, which depends fundamentally on the type and concentration of the electrolyte and the nature of the substrate [9,10], a phenomenon known as anodic spark deposition (ASD) takes place, whereby electrical arcs are established in the anode surface causing high energy density (current density of around 10^4 A cm^{-2}, reaching temperatures near to 8000 K). This allows to obtain porous and crystalline coatings of large surface area and from few tens to hundreds of micrometers thick [4,11,12]. The variation of the parameters of synthesis, i.e., the cell voltage, the current density, the nature and concentration of the electrolyte, the temperature, etc., allows to change the morphology and the proportion of the crystalline phases (anatase/rutile) of the coating formed on the anode [8,11,13–15], thereby modifying the photocatalytic activity [16–19].

Chromium is a metal with multiple industrial and technological applications, e.g., metallurgy, electroplating, textile industry, leather tanning, wood preservation, etc., and, consequently, it is a frequent contaminant in wastewaters. From the two main stable forms, Cr(VI) and Cr(III), the former is environmentally important due to its toxicity and its high solubility and mobility, recognized as a well-known human carcinogen that may cause dramatic effects to human health. On the other hand, Cr(III) is considered nontoxic and its mobility is lower than that of Cr(VI). For this reason, reduction of Cr(VI) to Cr(III) is the most used way to eliminate chromium pollution from waters [20]. Particularly, the photocatalytic reduction of Cr(VI) in water has been widely reported in several reviews in the literature as an environmentally friendly process for the treatment of this pollutant, and as a very simple system to evaluate the photocatalytic activity of various materials (see e.g. Refs. [21–25] and Refs. therein). Cr(VI) photocatalytic reduction has very important features that makes the system useful for this task: it is a very much studied model photocatalytic system, Cr(VI) concentration is very simple to be followed, the reaction in the presence of an organic donor such as EDTA or citric acid is rather fast, and it is the only reported metal species whose reductive TiO_2-photocatalytic removal is not influenced by the presence of oxygen. This last feature contrasts with those of most metals, and makes the process very useful for technological applications.

In the present work, the anodic oxidation process was employed to obtain TiO_2 coatings, varying the range of current density and the electrolyte concentration to search the conditions that yielded a high photocatalytic activity for Cr(VI) reduction in the presence of EDTA.

2. Experimental

2.1. Material and methods

All chemicals were reagent grade and used without further purification. H_2SO_4 (Cicarelli, 95–98%), potassium dichromate (Merck), ethylenediaminetetraacetic acid (EDTA, Riedel de Haën AG, Seelze – Hannover) were used. All other reagents were of the highest available purity. Diphenylcarbazide (DFC, UCB), acetone (Anedra, 99.5%) and phosphoric acid (Biopack, 85%) were used. Deionized water (conductivity: 0.05 μS cm^{-1}) was used. pH adjustments were made with perchloric acid (Merck, 70–72%).

pH was determined with a PHM210 Meter Lab® (Radiometer Analytical) pH meter. For ultrasonication, a Cleanson (25 KHz) equipment, model CS-1109, was used. Magnetic stirring was performed with a Metrohm E-649 stirrer or with a Velp 15 multistirrer. For anodization, a JMB direct current source, model LPS360DD, was used.

Commercially pure titanium plates (Grade 2 according to ASTM B367), 3 × 2 cm^2 and 0.2 cm, were used as substrates.

2.2. Synthesis of the photocatalysts

2.2.1. Preparation of the substrates

Titanium plates were included in acrylic (Subiton) and mechanically polished with SiC abrasive papers (Köln) from #120 to #1500, followed by the use of diamond paste of 1 μm (Praxis) lubricated with ethylene glycol (Cicarelli) for 30 min in a home-made polishing machine (250 rpm). After that, the substrates removed from the acrylic were cleaned with detergent and water, sprayed with alcohol, and finally dried with hot air.

2.2.2. Anodic oxidation

The photocatalysts were synthesized by anodic oxidation applying direct current. First, constant current density was applied up to a cell voltage of 120 V, and then, constant voltage was applied in spark discharge conditions. Two Pt sheets were used as cathode, separated 5 cm from the titanium anode. H_2SO_4 was used as electrolyte. The process variables were current density (J) of galvanostatic stage (200–3000 A m^{-2}) and electrolyte concentration (1 and 4 M H_2SO_4). Evolution of voltage and current was recorded during the oxidation. Anodization time was 5 min, except for the sample made at 3000 A m^{-2}, which was anodized for 3 min. After oxidation, the samples were cleaned with detergent and water, sprayed with alcohol, and finally dried with hot air.

Some samples were submitted to a thermal treatment (TT) at 450 °C in air for 1 h in an electrical oven (Indef Model M05C3). The heating rate was 10 °C min^{-1} and the cooling down was made inside the oven.

The samples were labeled as follows: a letter *S* and a number, corresponding to the electrolyte (H_2SO_4) and its molar concentration; a letter *J* and a number, corresponding to the current density in A m^{-2}; the thermal treatments are indicated by the letters *TT* at the end of the label. For example, the specimen *S1J1200* was obtained using 1 M H_2SO_4 and a current density of 1200 A m^{-2}, without thermal treatment.

2.3. Photocatalyst characterization

The surface of the oxides was observed by scanning electron microscopy (SEM), using a Carl Zeiss Supra 40 equipment. The images of the surface were analyzed using the Image J software [26]. In an area of 12 μm^2, the contour of each pore edge was marked. An equivalent diameter was calculated considering that the pores were circular, and an average pore diameter was calculated. The percentage of area covered by the pores, named as porous fraction, was calculated as the sum of the area of pores divided by the total image area.

A focused ion beam with SEM (FIB-SEM, FEI Helios NanoLab 650) was used for ion milling and measurement of the coating thickness. To minimize ion beam damage, a protective Pt layer (~1 μm thick) was deposited *in situ* using the electron source, prior to ion milling. The oxide thickness was obtained averaging ten measurements for each coating.

The crystalline structure of the oxides was identified by the glancing incidence X-ray diffraction (GI-XRD) technique with a glancing angle of 1° (Panalytical, Empyrean, Pixel3D detector), using CuK_α radiation at a step of 0.02° (2θ)/0.5 s. The accelerating voltage and the applied current were 40 kV and 30 mA, respectively.

The UV–Vis diffuse reflectance spectra (DRS) of the samples

were obtained using an UV–Vis–NIR spectrophotometer (Shimadzu, UV-3600) equipped with an integrating sphere. $BaSO_4$ was used as the reference. The spectra were recorded at room temperature in air and were used to obtain the bandgap value for the samples through Tauc plots [27].

2.4. Photocatalytic tests

A 0.4 mM $K_2Cr_2O_7$ aqueous solution containing 1 mM EDTA as a sacrificial synergetic agent was used. The initial pH was adjusted to 2. The photocatalyst samples were immersed into 10 mL of this solution contained in cylindrical glass reactors (36 mm diameter and 50 mm high) under magnetic stirring and were irradiated simultaneously using an artificial UV source (BLV MHL-404 lamp). An air flux was used to refrigerate the system. A water filter and a glass filter were located between the UV irradiation source and the reactor to remove IR radiation and UV wavelengths lower than 300 nm, respectively. The mean UV irradiance was 3700 μW cm^{-2}, measured at 365 nm with a Spectroline model DM-365 XA radiometer.

Prior to irradiation, solutions with the TiO_2 plates were kept in the dark for 30 min, to assure substrate-surface equilibrium. No significant changes in the concentration of Cr(VI) were observed after this dark period. Once the irradiation was initiated, 50 μL samples were taken each hour and diluted in 3 mL of water for analysis. Changes in Cr(VI) concentration were monitored through the DFC method at 540 nm [28]. For spectrophotometric measurements, a Hewlett-Packard diode array UV–visible spectrophotometer, model HP 8453 A, was employed. An error of 5% was taken for all photocatalytic experiments. The homogeneous photoreduction (absence of the photocatalyst) of Cr(VI) in the presence of EDTA was indicated as the blank. A sample of supported P25 prepared as described in Kleiman et al. [29] was used as reference.

3. Results and discussion

3.1. Preparation of the coatings

The temporal evolution of voltage and current density of plates submitted to anodic oxidation are shown in Figs. 1 and 2, respectively. Solid and dashed lines were used for the coatings prepared with 1 and 4 M H_2SO_4, respectively. Different colors identify the current density.

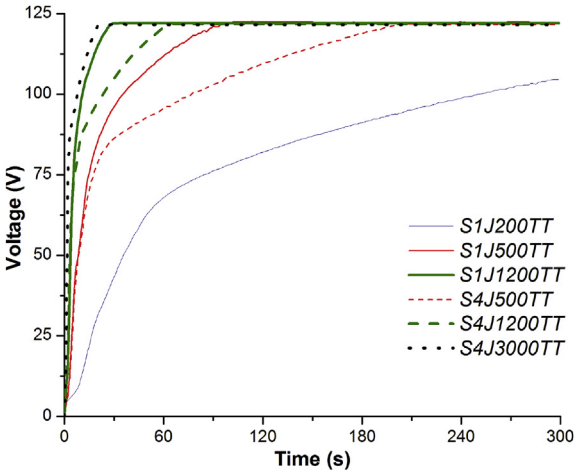

Fig. 1. Evolution of voltage during the anodic oxidation of Ti plates. Solid lines: *S1* samples; dashed lines: *S4* samples.

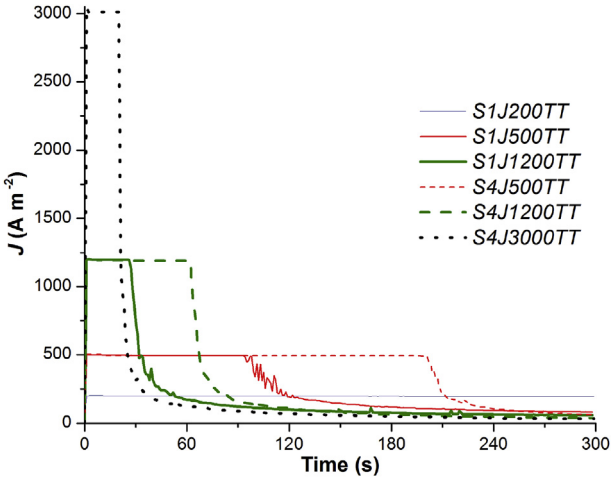

Fig. 2. Evolution of current density during the anodic oxidation of Ti plates. Solid lines: *S1* samples; dashed lines: *S4* samples.

Figs. 1 and 2 show the characteristic behavior of a galvanostatic-potentiostatic anodization process [8,11], in which a competition is established between the reactions of oxide dissolution and anodic growth of the coating [30]. The fluctuations in current density observed in Fig. 2 could be the result of a substrate-oxidation-breaking cycle produced by the spark discharge [31].

The anodization time required to reach 120 V decreased with the increase of the current density and increased at higher H_2SO_4 concentration, due to an increase in the electron flow and in the electrolyte conductivity, respectively [8,32].

3.2. Characterization of the coatings

The synthesized photocatalysts were characterized by SEM, FIB-SEM, GI-XRD and DRS techniques.

The SEM micrographs of the anodic oxides are shown in Fig. 3.

All micrographs show pores (dark gray) homogenously distributed on the surface, with raised edges (crater-like), typical of ASD coatings [4]. This morphology evidences that the formation of porous structures is due to the evolution of oxygen. In fact, from ~50 V up, a constant bubbling on the anode surface was observed. It is important to note that the *S4J3000TT* sample was anodized only for 3 min due to drawbacks in cell contacts, as the result of the severe anodization conditions. Nevertheless, this sample also presented a porous morphology (Fig. 3(f)).

On the other hand, the micrograph of *S1J200TT* shows "valleys" where the material did not show porosity, which can be explained by a lower final voltage (i.e., with a less energetic spark) reached after 5 min of anodization compared with the voltage reached for the other samples (see Fig. 1) [33].

It is seen that an increase of electrolyte concentration creates oxides with larger pores and a more intricate morphology, with a larger porous fraction (cf. Fig. 3 (a), (b), (c) and (d), (e), (f)). Table 1 summarizes the characteristic of the synthesized coatings. The current density seems to have little influence on the average pore diameter and there is no consistent influence on the porous fraction (Table 1). It has been reported that the use of high H_2SO_4 concentrations causes the creation of nanosized pores, together with an increase of the surface area [19]. The TT did not affect either the morphology of the oxides.

The thickness of selected coatings was analyzed to test the influence of the electrolyte concentration. FIB-SEM micrographs are

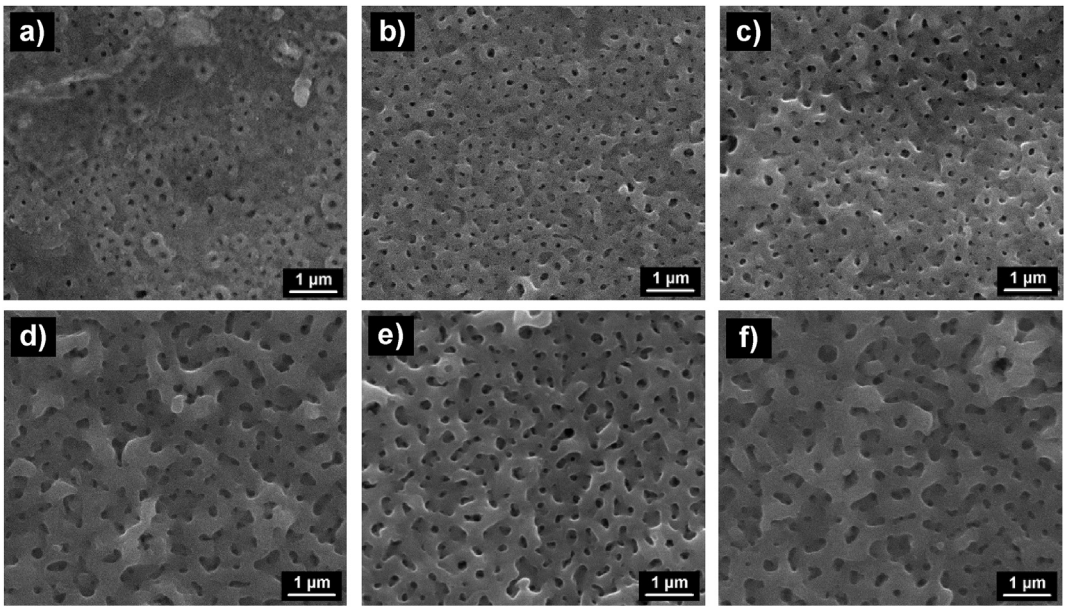

Fig. 3. SEM micrographs of synthesized coatings. a) *S1J200TT*; b) *S1J500TT*; c) *S1J1200TT*; d) *S4J500TT*; e) *S4J1200TT*; f) *S4J3000TT*.

Table 1
Summary of the characterization of coatings, zero order kinetic constant associated to the heterogeneous photocatalytic process (k_0) calculated with Eq. (2) and percentage of Cr(VI) removal in the presence of EDTA at 300 min (conditions of Fig. 6). The value of $k_1 = 2.60 \times 10^{-3}$ min^{-1} obtained for the homogeneous photoreduction reaction was taken for all the kinetic heterogeneous processes.

Sample	Average pore diameter (nm)	Porous fraction (%)	Anatase fraction	Bandgap (eV)	$k_0 \times 10^3$ (min^{-1})	R^2	% Cr(VI) removal
Blank	–	–	–	–	–	0.990	52.6
P25	–	–	0.78[a]	3.08[a]	0.79	0.998	69.9
S1J200TT	110	3.71	0.93	3.36	0.63	0.947	59.0
S1J500TT	95	6.54	0.80	3.13	1.50	0.978	78.9
S1J1200TT	101	4.59	0.74	3.12	1.67	0.958	86.6
S4J500TT	162	9.39	0.52	3.03	1.78	0.968	81.3
S4J1200TT	146	9.04	0.61	3.01	2.02	0.966	89.1
S4J3000TT	153	7.27	0.65	3.04	1.66	0.967	82.1

[a] According to ref. [34].

shown in Fig. 4.

The average coating thicknesses for the samples anodized in 1 M H_2SO_4 were 683 and 508 nm (Fig. 4 (a) and (b), respectively), while for samples anodized in 4 M H_2SO_4 they were 1458 and 1085 nm (Fig. 4 (c) and (d), respectively) showing that the increase of the electrolyte concentration produces thicker oxides, in agreement with literature data [19].

Diffractograms of the samples are shown in Fig. 5. The samples

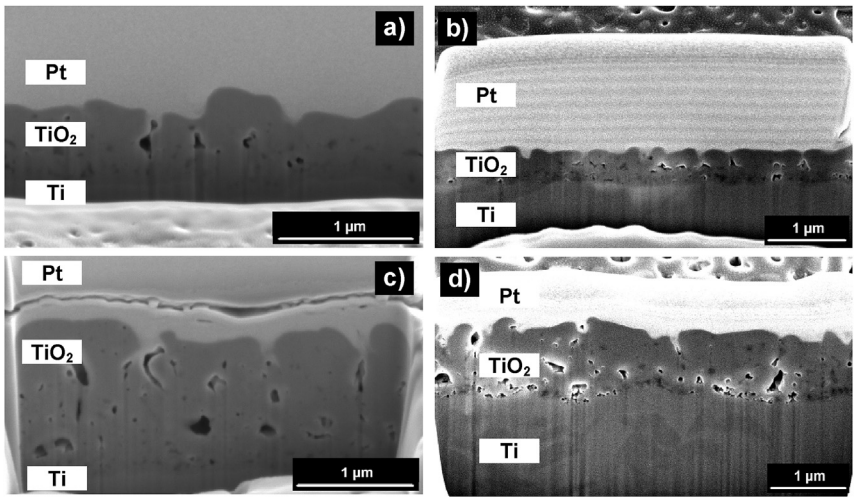

Fig. 4. FIB-SEM micrographs. a) *S1J500TT*; b) *S1J1200TT* c) *S4J500TT*; d) *S4J1200TT*.

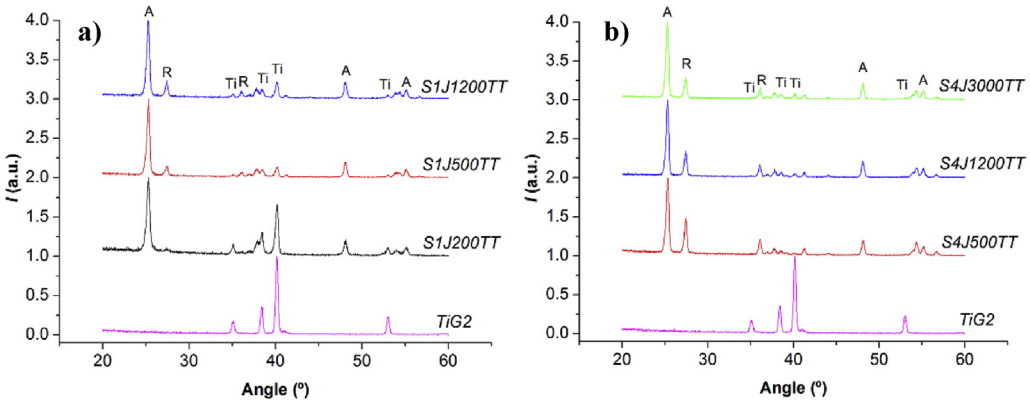

Fig. 5. Normalized diffractograms of synthesized coatings. a) *S1* samples; b) *S4* samples. A: anatase; R: rutile; Ti: titanium (substrate).

oxidized with the same current density are identified by the same color.

The increase of the electrolyte concentration produced a reduction in the intensity of the titanium peak (Ti) (cf. Fig. 5 (a) and (b)) as a result of an increase in the coating thickness [19]. This result is coherent with the average thickness values obtained from FIB-SEM micrographs, which increase at the most concentrated electrolyte solution (see Fig. 4).

The anatase fraction was calculated using the equation:

$$X_A = 1/[1 + 2.18(I_R/I_A)] \pm 2\% \quad (1)$$

where X_A is the molar fraction of anatase, and I_A and I_R are the total areas of the peaks of the X-ray intensities of the anatase and rutile strongest peaks, (101) and (110), respectively [35]. The results are summarized in Table 1.

An increase in the crystalline anatase fraction with the decrease of the electrolyte concentration was found, as indicated previously [19]. However, the influence of the current density is not clear in this case: for 4 M H_2SO_4, an increase in current density increased the anatase fraction [8], whereas 1 M H_2SO_4 has an opposite behavior [4].

The diffuse reflectance spectra were used to calculate the bandgap of the different photocatalysts presented in Table 1 (additional data are provided in the Supporting Information), using Tauc plots (E_g obtained by extrapolating to zero a linear fit of a plot of $(khv)^{1/2}$ against hv, as reported in Ref. [27]). The bandgap was lower than the expected for the anatase fraction found in each sample; this could be explained by the changes in the chemical and structural composition of coatings due to sulfur incorporation induced by spark [36]. However, the values of bandgaps of the 1 M H_2SO_4 samples should be taken carefully considering the coating thickness (<1 μm), due to the possible influence of the substrate on the obtained spectra [37].

3.3. Photocatalytic tests

The photocatalytic activity of the blank, the supported P25 and the anodic samples submitted to the TT were evaluated with the Cr(VI)/EDTA system in the conditions of similar experiments performed on other coatings [29]. Temporal profiles of normalized Cr(VI) concentration are presented in Fig. 6. The Cr(VI) conversion data of coatings were adjusted with a model that includes a first order kinetic constant (k_1) associated with the homogeneous photoreduction reaction (blank) and a zero order kinetic constant (k_0) associated with the heterogeneous photocatalytic process over the supported catalyst. This model was previously employed by

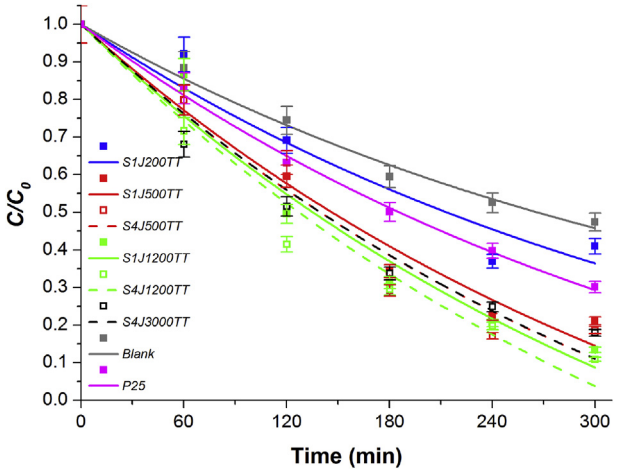

Fig. 6. Temporal evolution of normalized Cr(VI) concentration in photocatalytic experiments of Cr(VI) transformation in the presence of EDTA under UV irradiation performed with different TiO_2 coatings. Conditions: $[Cr(VI)]_0$ = 0.8 mM; [EDTA]/[Cr(VI)] = 1.25; pH 2; E = 3700 μW cm^{-2}. The adjusted curve of *S4J3000TT* is superimposed to the adjusted curve of *S4J500TT*. Solid lines and filled points: *S1* samples, P25 and blank; dashed lines and hollow points: *S4* samples.

Kleiman et al. [29] and can be described by equation (2):

$$\frac{C}{C_0} = \left(1 + \frac{k_0}{k_1}\right) e^{-k_1 t} - \frac{k_0}{k_1} \quad (2)$$

where C is the Cr(VI) concentration in the solution sampled each hour, C_0 is the Cr(VI) concentration at the beginning of the photocatalytic test, k_1 is the kinetic constant for the homogeneous process and k_0 is the kinetic constant of the photocatalytic reaction. The k_1 value obtained for the blank ($k_1 = 2.60 \times 10^{-3}$ min^{-1}; $R^2 = 0.98$) was used to adjust the curves of the immobilized catalysts. The k_0 and R^2 values for the samples are summarized in Table 1.

The transformation of Cr(VI) over the TiO_2 samples was faster than the obtained through the homogeneous photochemical reaction. The maximal transformation for the 5 h of irradiation time (89.1%) was obtained with the *S4J1200TT* sample. According to the values of k_0 in Table 1, the photocatalytic activity follows the order *S4J1200TT* > *S4J500TT* > *S1J1200TT* > *S4J3000TT* > *S1J500TT* > *S1J200TT*. The comparison with the P25 sample [29] indicates that all the new samples (except *S1J200TT*) exhibit a higher photocatalytic activity (Fig. 6 and Table 1), although the comparison is not direct since this sample is not prepared similarly to the anodic ones,

and the amount of TiO_2 present in the anodic coatings is not known. The relationship between higher anodization voltages and higher activities for TiO_2 anodic coatings has been observed by Brunella et al. for stearic acid degradation [16], and by Wang et al. for methyl orange oxidation [17].

Comparing the activities of samples obtained with the same current density but different electrolyte concentrations (i.e., *S1J500TT* vs. *S4J500TT* and *S1J1200TT* vs. *S4J1200TT*), the best photocatalytic performance was obtained with samples synthesized in the most concentrated electrolyte (4 M), and this could be the result of a higher pore diameter, a higher film thickness, the light penetration depth [38,39] and the anatase fraction (see below). It has been described previously (Fig. 3) that the use of a higher electrolyte concentration increases the quantity and diameter of pores, improving the accessibility of the solution to the internal surface of the pores, and then increasing the effectively irradiated and active area for adsorption and photocatalysis [17,19].

Comparing now the activities of samples obtained with the same electrolyte concentration but using different current densities (i.e., *S1J500TT* vs. *S1J1200TT* and *S4J500TT* vs. *S4J1200TT*), the best photocatalytic performance corresponded to the samples obtained with the highest current density (1200 A m^{-2}) which produced coatings with an anatase fraction near to an optimum, as described in the next paragraph.

A relationship between the anatase fraction and the photocatalytic activity was found for samples with TT (excluding *S4J3000TT* due to its lower anodization time), which was very well fitted through a quadratic equation ($R^2 = 0.98$), as shown in Fig. 7.

According to the adjusted curve, the maximum for the photocatalytic activity appears at an anatase fraction close to 0.65. This result is consistent with others that indicate that a synergetic effect exists between both crystalline phases due to separation of charges, caused by photogenerated electrons in rutile that could migrate to the conduction band of anatase suppressing recombination. This synergetic effect was observed in a range from 40 to 80% anatase, with an optimum value about 60% [40–43], as that obtained here.

As observed in Figs. 6 and 7, the least active sample for Cr(VI) reduction was *S1J200TT*, and this can be explained considering that the amount of rutile to assist electron-hole separation is probably insufficient [41]. This sample exhibits also a low porous fraction (Table 1).

In Fig. 8, diffractograms of samples with and without TT are presented, showing that the TT does not modify the proportion of crystalline phases of the coatings. This could be due to the anodization conditions above spark voltage, which generates high local current densities and temperatures, inducing the formation of crystalline oxides (anatase and rutile) without further effect of the applied TT [8,11].

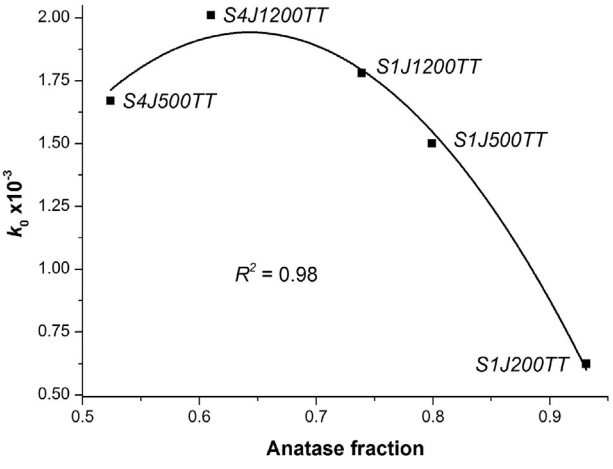

Fig. 7. Relationship between the photocatalytic activity and the anatase fraction for samples with TT.

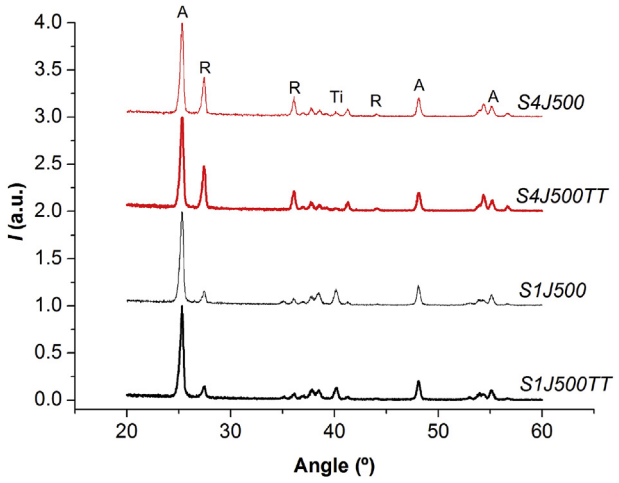

Fig. 8. Diffractograms of samples with (thick trace) and without (fine trace) TT.

In Fig. 9, a comparison of the photocatalytic activity of samples with and without TT is presented. *S1J500* and *S4J500* samples (without TT) showed a lower photocatalytic activity than those of the same samples with TT, indicating that although the morphology and proportion of the crystalline phases of the coatings is not modified, the TT would increase the crystallinity of the oxides, and thus the photocatalytic activity. Masahashi et al. [19] explained the better photocatalytic activity of annealed anodic oxides (TT samples) by a reduction of the lattice strain. Low inhomogeneous strains involve reduction of crystal lattice defects like dislocation and vacancy, which become recombination centers of the photogenerated electron and hole, thus decreasing activity.

As it is observed in Fig. 9, the effect of TT is more perceptible in *S1J500* than in *S4J500*, because a higher electrolyte concentration and conductivity induce the formation of more crystalline oxides [8] and a higher rutile content.

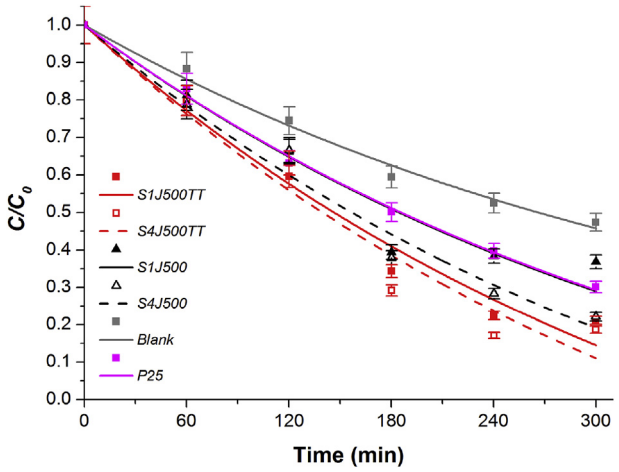

Fig. 9. Temporal evolution of normalized Cr(VI) concentration in photocatalytic experiments of Cr(VI) transformation in the presence of EDTA under UV irradiation performed with different TiO_2 coatings, with and without TT. Conditions: $[Cr(VI)]_0$ = 0.8 mM; [EDTA]/[Cr(VI)] = 1.25; pH 2; E = 3700 μW cm^{-2}. Solid lines and filled points: *S1* samples, P25 and blank; dashed lines and hollow points: *S4* samples.

4. Conclusions

Different porous TiO_2 coatings prepared by anodic oxidation of Ti plates have been prepared. The influence of the electrolyte concentration, the current density and the thermal treatment on the morphology, the crystalline phases and the photocatalytic activity of the new porous TiO_2 coatings was evaluated.

A clear influence of the electrolyte concentration on the morphology of the coatings was found and it has been attributed to the increase of the pore diameter, the porous fraction and the thickness of the synthesized coatings. On the other hand, the current density and the thermal treatment seem to have no influence on the morphology.

The photocatalytic activity over this type of TiO_2 coatings was analyzed for the first time with a reductive TiO_2 photocatalytic system, Cr(VI) in the presence of EDTA. The activity of the coatings was found to increase with the H_2SO_4 concentration and with the current density, which was attributed mainly to the anatase/rutile ratio, the porous size and the porous fraction. The maximal photocatalytic activity of the coatings was found close to an anatase fraction of 0.65.

The high photocatalytic activity of these coatings, which, in some cases, is better than that of P25, makes them potential materials useful for applications in heterogeneous photocatalysis processes for water and wastewater treatment.

Acknowledgements

This work was supported by Agencia Nacional de Promoción Científica y Tecnológica (ANPCyT) from Argentina under PICT-2011-0463, PICT-2011-1378 and PICT-2012-2952 grants. The authors wish to thank Adriana Domínguez from the Microscopy Materials Laboratory and Daniel Vega from the DRX Laboratory, Department of Condensed Matter Physics, both from CAC-CNEA, Gustavo Giménez from Micro and Nano Electronics of Bicentennial Center from INTI for the FIB-SEM micrographs and Enrique San Román from INQUIMAE-UBA for the DRS.

Appendix A. Supplementary data

Supplementary data related to this article can be found at http://dx.doi.org/10.1016/j.matchemphys.2017.01.034.

References

[1] A. Fujishima, X. Zhang, Titanium dioxide photocatalysis: present situation and future approaches, Comptes Rendus Chim. 9 (5) (2006) 750–760.
[2] C.H. Kwon, H. Shin, J.H. Kim, W.S. Choi, K.H. Yoon, Degradation of methylene blue via photocatalysis of titanium dioxide, Mater. Chem. Phys. 86 (1) (2004) 78–82.
[3] L. Zhang, R. Dillert, D. Bahnemann, M. Vormoor, Photo-induced hydrophilicity and self-cleaning: models and reality, Energy & Environ. Sci. 5 (6) (2012) 7491–7507.
[4] M.V. Diamanti, M. Ormellese, M. Pedeferri, Application-wise nanostructuring of anodic films on titanium: a review, J. Exp. Nanosci. 10 (17) (2015) 1285–1308.
[5] Y. Mizukoshi, N. Masahashi, Photocatalytic activities and crystal structures of titanium dioxide by anodization: their dependence upon current density, Mater. Trans. 51 (8) (2010) 1443–1448.
[6] Y.J. Park, K.H. Shin, H.J. Song, Effects of anodizing conditions on bond strength of anodically oxidized film to titanium substrate, Appl. Surf. Sci. 253 (14) (2007) 6013–6018.
[7] X. Cui, H.M. Kim, M. Kawashita, L. Wang, T. Xiong, T. Kokubo, T. Nakamura, Preparation of bioactive titania films on titanium metal via anodic oxidation, Dent. Mater. 25 (1) (2009) 80–86.
[8] M.V. Diamanti, M.P. Pedeferri, Effect of anodic oxidation parameters on the titanium oxides formation, Corros. Sci. 49 (2) (2007) 939–948.
[9] J.M. Albella, I. Montero, J.M. Martinez-Duart, V. Parkhutik, Dielectric breakdown processes in anodic Ta_2O_5 and related oxides, J. Mater. Sci. 26 (13) (1991) 3422–3432.
[10] A.I. Kociubczyk, M.L. Vera, C.E. Schvezov, E. Heredia, A.E. Ares, TiO_2 coatings in alkaline electrolytes using anodic oxidation technique, Procedia Mater. Sci. 8 (2015) 65–72.
[11] H.J. Song, S.H. Park, S.H. Jeong, Y.J. Park, Surface characteristics and bioactivity of oxide films formed by anodic spark oxidation on titanium in different electrolytes, J. Mater. Process. Technol. 209 (2) (2009) 864–870.
[12] N.K. Kuromoto, R.A. Simão, G.A. Soares, Titanium oxide films produced on commercially pure titanium by anodic oxidation with different voltages, Mater. Charact. 58 (2) (2007) 114–121.
[13] H.D. Traid, M.L. Vera, A.E. Ares, M.I. Litter, Porous titanium dioxide coatings obtained by anodic oxidation for photocatalytic applications, Procedia Mater. Sci. 9 (2015) 619–626.
[14] A.F. Yetim, Investigation of wear behavior of titanium oxide films, produced by anodic oxidation, on commercially pure titanium in vacuum conditions, Surf. Coat. Technol. 205 (6) (2010) 1757–1763.
[15] H.D. Traid, M.L. Vera, A.E. Ares, M.I. Litter, Obtención de recubrimientos porosos de TiO_2 por oxidación anódica para aplicaciones fotocatalíticas, Av. Ciencias Ing. 7 (1) (2016) 19–25.
[16] M.F. Brunella, M.V. Diamanti, M.P. Pedeferri, F. Di Fonzo, C.S. Casari, A.L. Bassi, Photocatalytic behavior of different titanium dioxide layers, Thin Solid Films 515 (16) (2007) 6309–6313.
[17] M.R. Bayati, F. Golestani-Fard, A.Z. Moshfegh, The effect of growth parameters on photo-catalytic performance of the MAO-synthesized TiO_2 nano-porous layers, Mater. Chem. Phys. 120 (2) (2010) 582–589.
[18] W. Wang, J. Tao, T. Wang, L. Wang, Photocatalytic activity of porous TiO_2 films prepared by anodic oxidation, Rare Met. 26 (2) (2007) 136–141.
[19] N. Masahashi, Y. Mizukoshi, S. Semboshi, N. Ohtsu, Enhanced photocatalytic activity of rutile TiO_2 prepared by anodic oxidation in a high concentration sulfuric acid electrolyte, Appl. Catal. B Environ. 90 (1) (2009) 255–261.
[20] R. Djellabi, F.M. Ghorab, S. Nouacer, S. Abdelaziz, O. Khireddine, Cr(VI) photocatalytic reduction under sunlight followed by Cr(III) extraction from TiO_2 surface, Mater. Lett. 176 (2016) 106–109.
[21] M.I. Litter, Heterogeneous photocatalysis: transition metal ions in photocatalytic systems, Appl. Catal. B Environ. 23 (2) (1999) 89–114.
[22] M.I. Litter, Treatment of chromium, mercury, lead, uranium, and arsenic in water by heterogeneous photocatalysis, Adv. Chem. Eng. 36 (2009) 37–67.
[23] M.I. Litter, N. Quici, New advances in heterogeneous photocatalysis for treatment of toxic metals and arsenic, Nanomater. Environ. Prot. (2014) 143–167.
[24] M.I. Litter, Mechanisms of removal of heavy metals and arsenic from water by TiO_2-heterogeneous photocatalysis, Pure Appl. Chem. 87 (6) (2015) 557–567.
[25] M.I. Litter, N. Quici, J.M. Meichtry, A.M. Senn, Photocatalytic removal of metallic and other inorganic pollutants, in: D.D. Dionysiou, G. Li Puma, J. Ye, J. Schneider, D. Bahnemann (Eds.), Photocatalysis: Applications, 2016, pp. 35–71, http://dx.doi.org/10.1039/9781782627104-00035. Royal Society, Ch. 2.
[26] W.S. Rasband, ImageJ, US National Institute of Health, Bethesda, Maryland, USA, 1997–2014. http://imagej.nih.gov/ij/.
[27] A.B. Murphy, Band-gap determination from diffuse reflectance measurements of semiconductor films, and application to photoelectrochemical water-splitting, Sol. Energy Mater. Sol. Cells 91 (14) (2007) 1326–1337.
[28] ASTM D1687-12. Standard Test Methods for Chromium in Water. A-photometric Diphenyl-carbohydrazide.
[29] A. Kleiman, A. Márquez, M.L. Vera, J.M. Meichtry, M.I. Litter, Photocatalytic activity of TiO_2 thin films deposited by cathodic arc, Appl. Catal. B Environ. 101 (3) (2011) 676–681.
[30] V. Zwilling, E. Darque-Ceretti, A. Boutry-Forveille, D. David, M.Y. Perrin, M. Aucouturier, Structure and physicochemistry of anodic oxide films on titanium and TA6V alloy, Surf. Interface Anal. 27 (7) (1999) 629–637.
[31] M.L. Vera, Obtención y caracterización de películas hemocompatibles de TiO_2, PhD Thesis in Science and Technology, Instituto Sábato. CNEA-UNSAM, Buenos Aires, 2013. Chap. 6, www.isabato.edu.ar/resumenDM.asp?pp=0&cod=IS/TD71/13.
[32] A.K. Sharma, Anodizing titanium for space applications, Thin Solid Films 208 (1) (1992) 48–54.
[33] S. Komiya, K. Sakamoto, N. Ohtsu, Structural changes of anodic layer on titanium in sulfate solution as a function of anodization duration in constant current mode, Appl. Surf. Sci. 296 (2014) 163–168.
[34] M.L. Vera, Preparación de fotocatalizadores de TiO_2 soportados para su uso en potabilización de aguas, Master Thesis in Materials Science and Technology, Instituto Sábato. CNEA-UNSAM, Buenos Aires, 2008. Chap. IV, http://www.isabato.edu.ar/resumenPM.asp?pp=1&cod=IS/T–112/08.
[35] J. Criado, C. Real, Mechanism of the inhibiting effect of phosphate on the anatase → rutile transformation induced by thermal and mechanical treatment of TiO_2, J. Chem. Soc. Faraday Trans. 1 Phys. Chem. Condens. Phases 79 (12) (1983) 2765–2771.
[36] J.F. Vanhumbeeck, J. Proost, Current understanding of Ti anodisation: functional, morphological, chemical and mechanical aspects, Corros. Rev. 27 (3) (2009) 117–204.
[37] Y. Mizukoshi, N. Ohtsu, S. Semboshi, N. Masahashi, Visible light responses of sulfur-doped rutile titanium dioxide photocatalysts fabricated by anodic oxidation, Appl. Catal. B Environ. 91 (1) (2009) 152–156.
[38] C.B. Marien, T. Cottineau, D. Robert, P. Drogui, TiO_2 Nanotube arrays: influence of tube length on the photocatalytic degradation of Paraquat, Appl. Catal. B Environ. 194 (2016) 1–6.
[39] W. Choi, S.J. Hong, Y.S. Chang, Y. Cho, Photocatalytic degradation of

polychlorinated dibenzo-p-dioxins on TiO_2 film under UV or solar light irradiation, Environ. Sci. Technol. 34 (22) (2000) 4810–4815.
[40] D.C. Hurum, A.G. Agrios, K.A. Gray, T. Rajh, M.C. Thurnauer, Explaining the enhanced photocatalytic activity of Degussa P25 mixed-phase TiO_2 using EPR, J. Phys. Chem. B 107 (19) (2003) 4545–4549.
[41] D.O. Scanlon, C.W. Dunnill, J. Buckeridge, S.A. Shevlin, A.J. Logsdail, S.M. Woodley, C.R.A. Catlow, M.J. Powell, R.G. Palgrave, I.P. Parkin, G.W. Watson, Band alignment of rutile and anatase TiO_2, Nat. Mater. 12 (9) (2013) 798–801.
[42] R. Su, R. Bechstein, L. Sø, R.T. Vang, M. Sillassen, B. Esbjörnsson, A. Palmqvist, F. Besenbacher, How the anatase-to-rutile ratio influences the photoreactivity of TiO_2, J. Phys. Chem. C 115 (49) (2011) 24287–24292.
[43] T. Luttrell, S. Halpegamage, J. Tao, A. Kramer, E. Sutter, M. Batzill, Why is anatase a better photocatalyst than rutile? -Model studies on epitaxial TiO_2 films, Sci. Rep. 4 (2014).